International Journal of Fracture

The steady-state Archard adhesive wear problem revisited based on the phase field approach to fracture

--Manuscript Draft--

Manuscript Number:	
Full Title:	The steady-state Archard adhesive wear problem revisited based on the phase field approach to fracture
Article Type:	Original Research
Keywords:	Adhesive wear; Steady-state conditions; Phase field; Finite element method
Corresponding Author:	Valerio Carollo Universita degli Studi di Trento Trento, ITALY
Corresponding Author Secondary Information:	
Corresponding Author's Institution:	Universita degli Studi di Trento
Corresponding Author's Secondary Institution:	
First Author:	Valerio Carollo
First Author Secondary Information:	
Order of Authors:	Valerio Carollo
	Marco Paggi
	José Reinoso
Order of Authors Secondary Information:	
Funding Information:	Spanish Ministry of Economy and Competitiveness/FEDER (MAT2015-71036-P and MAT2015-71309-P) — Prof José Reinoso
	Andalusian Government (TEP- 7093 and P12-TEP-1050) — Prof José Reinoso
Abstract:	The problem of adhesive wear is herein investigated in relation to periodic asperity junction models in the framework of the Archard interpretation suggesting that wear debris formation is the result of asperity fracture. To this aim, the Phase Field model for fracture is exploited to simulate the crack pattern leading to debris formation in the asperity junction model. Based on dimensional analysis considerations, the effect of the size of the junction length, the lateral size of the asperity, and the amplitude of the re-entrant corner angles γ and β defined by the junction geometry is examined in the parametric analysis. Results show that two failure modes are expected to occur, one with a crack nucleated at the re-entrant corner γ, and another with a crack nucleated at the re-entrant corner β, depending on the dominant power of the stress-singularity at the two re-entrant corner tips. Steady-state adhesive wear, where the initial asperity junction geometry is reproduced after debris formation, is observed for asperity junctions with $\gamma = 45^\circ$, almost independently of the lateral size of the asperity and of the horizontal projection of the junction length.
Suggested Reviewers:	Jim Barber Professor, University of Michigan jbarber@umich.edu
	David Hills Professor, University of Oxford david.hills@eng.ox.ac.uk
	Daniele Dini

	Professor, Imperial College London d.dini@imperial.ac.uk

Noname manuscript No.
(will be inserted by the editor)

The steady-state Archard adhesive wear problem revisited based on the phase field approach to fracture

Valerio Carollo · Marco Paggi · José Reinoso

the date of receipt and acceptance should be inserted later

Abstract The problem of adhesive wear is herein investigated in relation to periodic asperity junction models in the framework of the Archard interpretation suggesting that wear debris formation is the result of asperity fracture. To this aim, the Phase Field model for fracture is exploited to simulate the crack pattern leading to debris formation in the asperity junction model. Based on dimensional analysis considerations, the effect of the size of the junction length, the lateral size of the asperity, and the amplitude of the re-entrant corner angles γ and β defined by the junction geometry is examined in the parametric analysis. Results show that two failure modes are expected to occur, one with a crack nucleated at the re-entrant corner γ, and another with a crack nucleated at the re-entrant corner β, depending on the dominant power of the stress-singularity at the two re-entrant corner tips. Steady-state adhesive wear, where the initial asperity junction geometry is reproduced after debris formation, is observed for asperity junctions with $\gamma = 45°$, almost independently of the lateral size of the asperity and of the horizontal projection of the junction length.

Keywords Adhesive wear · Steady-state conditions · Phase field · Finite element method

V. Carollo E-mail: valerio.carollo@imtlucca.it · M.Paggi
IMT School for Advanced Studies, Piazza San Francesco 19, 55100, Lucca (Italy)

J. Reinoso
Universidad de Sevilla, Avda. de los Descubrimientos s/n, E-41092, Seville (Spain)

1 Introduction

Adhesive wear is one of the various forms of wear of materials [24] and its development is not yet fully understood. It is mostly induced by severe adhesion between asperities of rough surfaces in contact. It has its roots at the micro-scale and it occurs under special environmental conditions [26]. Its clear observation is possible only in high vacuum, where there is no gas between the two surfaces in contact, and in absence of impurities like oxide films. In addition to the need for such particular conditions, adhesive wear can frequently occur in mechanical system components in contact with insufficient lubrication, as for plane bearings or gear teeth.

Adhesive wear can occur not only in metals, but also in ceramics and polymers. Materials with comparable

hardness are more prone to adhesive wear [3] and metals can develop the most severe form. In [31] it is theorized that when two metallic surfaces are sufficiently close to each other to consider them in contact, electrons can be exchanged between the two opposing surfaces. This free movement of the electrons could provide the explanation for the local bonds causing adhesive wear.

In the literature, the study of adhesive wear is mostly based on two well-known pioneering approaches: the atomistic model by Holm [13] and the continuum fracture model by Archard [2]. Holm's model assumes that adhesive wear is the result of atoms removal from the asperities in contact. Consequently, the asperities undergo a process of progressive flattening. This model is supported by experiments conducted with the atomic force microscope [27,10] and by molecular dynamics simulations [1,29]. However, Holm's model can hardly predict the occurrence of steady state wear configuration observed in many tribological systems [8], due to a progressive flattening of the surfaces which usually continues without reaching an asymptotic geometry.

Archard's model assumes that adhesive wear is the result of debris originated by asperity interlocking and fracture. This hypothesis is largely confirmed by many experimental evidences [11,5,6,14]. When two joint asperities are subjected to sliding motion, the asperities experience a strong deformation which causes severe plastic strain in ductile materials (Fig. 1 (a)). After that stage, cracks nucleate under shear (Fig. 1 (b)) until the fractured material leads to debris formation.

Most of the studies in the literature on adhesive wear are focused on the estimation of the debris volume (wear volume) [5], to quantify the material loss. In [15,12], for instance, the assumption of perfect adhesion is put forward for the case of complete contact

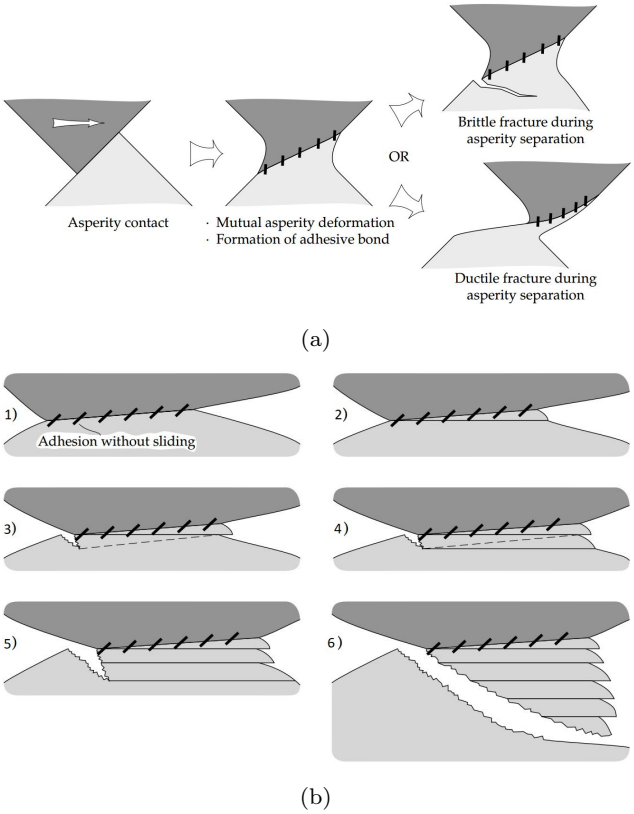

Fig. 1 Archard's model: (a) Deformation of the asperities before fracture; (b) shearing mechanism of fracture of the asperities. Images adopted from [26].

problems. In the present study, we propose a method to investigate on the stage of fracture which leads to debris formation. Using the phase field (PF) approach to fracture, whose features are described in Section 2, the nucleation of cracks at joined asperities can be simulated, along with the crack path resulting from their propagation. By performing a parametric study with different model asperity geometries, the conditions for the occurrence of a steady state wear are carefully analysed and identified, considering that steady state wear occurs when the geometrical features of the undeformed rough profile are re-generated after wear debris formation.

The manuscript is organized as follows: in Section 2, an insight on the PF approach o fracture is given

and the numerical simulations based on the PF model are described. In Section 3, the parametric analysis is presented and results are discussed. Finally, conclusions are provided in Section 5.

2 Proposed simulation method and design of numerical experiments

2.1 Phase Field approach to fracture

In this section we describe the thermodynamically consistent formulation of the Phase Field method for fracture. The formulation herein adopted is based on the approach proposed in [17,18] and revisited in relation to interface fracture in [22]. This formulation lays on the classical fracture theory of Griffith, but it models the crack as a diffuse damage process rather than a sharp discontinuity.

Our approach is developed on a two-dimensional framework (Fig. 2(a)). We consider an arbitrary body $\Omega \in \mathbb{R}^2$ in the Euclidean two-dimensional space. A point in the body Ω is defined by the vector of its Cartesian coordinates $\mathbf{x}$, while the body forces are denoted by $\mathbf{f}_v : \Omega \longrightarrow \mathbb{R}^2$. The boundaries of Ω are denoted by $\partial\Omega$, which in turn are split into the boundary $\partial\Omega_u$ where kinematic (Dirichlet) boundary conditions are prescribed and in the boundary $\partial\Omega_t$ where traction (Neumann) boundary conditions are imposed, being $\partial\Omega_t \cup \partial\Omega_u = \partial\Omega$ and $\partial\Omega_t \cap \partial\Omega_u = \emptyset$. For a generic point of Ω, we denote its displacement vector by $\mathbf{u}$ and the Cauchy stress tensor by $\boldsymbol{\sigma}$. Then, the prescribed displacements and tractions at the boundaries $\partial\Omega_u$ and $\partial\Omega_t$ are:

$$\mathbf{u} = \overline{\mathbf{u}} \quad \text{on } \partial\Omega_u \quad \text{and} \quad \overline{\mathbf{t}} = \boldsymbol{\sigma} \cdot \mathbf{n} \quad \text{on } \partial\Omega_t,$$

where $\mathbf{n}$ denotes the outward normal unit vector to the body.

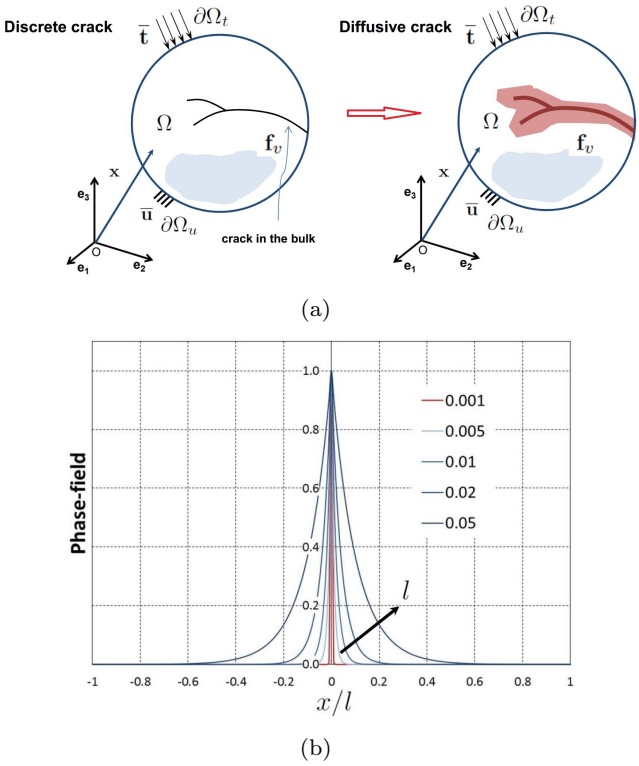

Fig. 2 (a) from the discrete discontinuity (left) to the smeared discontinuity (right) in the bi-dimensional framework; (b) 1D approximation function which smears out the discontinuity, where the damage $\mathfrak{d}$ follows the exponential based function $\mathfrak{d} = \mathrm{e}^{-|x|/l}$.

In the Phase Field approach to fracture, the crack, which is usually represented by a discrete discontinuity, is regularized through a diffusing scalar damage variable $\mathfrak{d}$, with $\mathfrak{d} : \Omega \times [0,t] \longrightarrow [0,1]$ [4]. For $\mathfrak{d} = 0$, the undamaged state takes place, while for $\mathfrak{d} = 1$ Griffith fracture occurs. Between 0 and 1, the damage has an exponential variation in space, as depicted for a 1D test problem of a bar in uniaxial tension in Fig. 2(b). The parameter l is the so-called Phase Field internal length scale, which controls the width of the damage zone [17, 18] around the crack identified by the level set $\mathfrak{d} = 1$.

Based on this framework, the total internal energy of the system takes the form:

$$\mathit{\Pi}(\mathbf{u},\mathfrak{d}) = \int_{\Omega} \psi(\boldsymbol{\varepsilon},\mathfrak{d})\,\mathrm{d}\Omega + \int_{\Omega} \mathcal{G}_c\gamma(\mathfrak{d},\nabla_{\mathbf{x}}\mathfrak{d})\,\mathrm{d}\Omega, \tag{1}$$

where $\psi(\boldsymbol{\varepsilon},\mathfrak{d})$ is the elastic strain energy density which depends on the damage variable $\mathfrak{d}$ and on the strain tensor $\boldsymbol{\varepsilon}$. $\mathcal{G}_c$ is the Griffith fracture energy and $\gamma(\mathfrak{d},\nabla_{\mathbf{x}}\mathfrak{d})$ is the so-called crack density functional which depends on $\mathfrak{d}$ and its gradient $\nabla_{\mathbf{x}}\mathfrak{d}$, which introduces a nonlocality in the formulation, essential to avoid mesh-dependency. The crack density functional herein considered is the same as that defined in [17]:

$$\gamma(\mathfrak{d},\nabla_{\mathbf{x}}\mathfrak{d}) = \frac{1}{2l}\mathfrak{d}^2 + \frac{l}{2}|\nabla_{\mathbf{x}}\mathfrak{d}|^2. \tag{2}$$

The Euler equations associated with the phase field formulation are:

$$\mathfrak{d} - l^2\nabla^2_{\mathbf{x}}\mathfrak{d} = 0 \quad \text{in } \Omega \quad \text{and} \quad \nabla_{\mathbf{x}}\mathfrak{d}\cdot\mathbf{n} = 0 \quad \text{in } \partial\Omega, \tag{3}$$

where $\nabla^2_{\mathbf{x}}\mathfrak{d}$ denotes the Laplacian of the damage variable.

Regarding the elastic energy stored in the body $\psi(\boldsymbol{\varepsilon},\mathfrak{d})$, the positive-negative split proposed in [16] is herein applied to distinguish between tension and compression stress states. Other variants fro the split are possible, see e.g. [9]. The positive elastic energy is a fraction of the total elastic energy and it depends on the tensile stresses, while the negative counterpart depends on the compressive ones. Hence, in formulae, the positive-negative split proposed in [16] takes the form:

$$\psi(\boldsymbol{\varepsilon},\mathfrak{d}) = \mathfrak{g}(\mathfrak{d})\psi^e_+(\boldsymbol{\varepsilon}) + \psi^e_-(\boldsymbol{\varepsilon}), \tag{4a}$$

$$\psi^e_+(\boldsymbol{\varepsilon}) = \frac{\lambda}{2}\left(\langle \mathrm{tr}[\boldsymbol{\varepsilon}]\rangle_+\right)^2 + \mu\mathrm{tr}[\boldsymbol{\varepsilon}^2_+], \tag{4b}$$

$$\psi^e_-(\boldsymbol{\varepsilon}) = \frac{\lambda}{2}\left(\langle \mathrm{tr}[\boldsymbol{\varepsilon}]\rangle_-\right)^2 + \mu\mathrm{tr}[\boldsymbol{\varepsilon}^2_-], \tag{4c}$$

where λ and μ are the Lamé constants, ε_+ and ε_- are, respectively, the positive and negative counterparts of the strain tensor. The symbol $\mathrm{tr}[\bullet]$ denotes the trace operator, the symbol $\langle\bullet\rangle_\pm$ denotes the so-called Macaulay brackets which describe the operation $\langle\bullet\rangle_\pm = (\bullet \pm |\bullet|)/2$. The function $\mathfrak{g}(\mathfrak{d})$ is a degradation function that is selected as:

$$\mathfrak{g}(\mathfrak{d}) = (1-\mathfrak{d})^2 + \mathcal{K}, \tag{5}$$

where $\mathcal{K}$ is a residual stiffness introduced to avoid numerical instabilities when $\mathfrak{d} = 1$. Note that in Eq. (4a) the degradation function (5) multiplies only the positive part of the elastic energy, thus avoiding damage growth in compression.

The split of the strain tensor into $(\boldsymbol{\varepsilon} = \boldsymbol{\varepsilon}_+ + \boldsymbol{\varepsilon}_-)$ is made according to the following spectral decomposition of the strain tensor:

$$\boldsymbol{\varepsilon}_\pm = \sum_{i=1}^{n_{dim}} \langle\varepsilon^i\rangle_\pm \mathbf{n}^i_\varepsilon \otimes \mathbf{n}^i_\varepsilon, \tag{6}$$

where ε^i and $\mathbf{n}^i_\varepsilon$ are, respectively, the eigenvalues and the eigenvectors of the strain tensor.

Finally, the Cauchy stress tensor of the Phase Field formulation takes the form:

$$\boldsymbol{\sigma} := \frac{\partial\hat{\psi}}{\partial\boldsymbol{\varepsilon}} = \mathfrak{g}(\mathfrak{d})\boldsymbol{\sigma}_+ + \boldsymbol{\sigma}_-; \tag{7}$$
$$\text{with } \boldsymbol{\sigma}_\pm = \lambda\left(\langle\mathrm{tr}[\boldsymbol{\varepsilon}]\rangle_\pm\right)\mathbf{1} + 2\mu\boldsymbol{\varepsilon}_\pm,$$

where $\mathbf{1}$ denotes the second-order identity tensor, and $\boldsymbol{\sigma}_\pm$ denotes the positive-negative counterpart of the stress tensor.

This formulation has been implemented by the present authors as a 4-node finite element with the isoparametric formulation in the finite element research program FEAP [30], see [22] for a detailed definition of all the

operators for a monolithic fully implicit solution strategy of the nonlinear problem.

2.2 Design of the numerical experiments

The geometry of rough profiles in contact has been herein simplified by considering triangular asperities with a periodic distribution along the profile, inspired by the model asperity studied in [5]. Each asperity has one side in contact with another, as shown in Fig. 3 (a). Taking advantage of periodicity, only the representative unit asperity junction is investigated (Fig. 3 (b)), with periodic boundary conditions imposed on the vertical sides of the unit asperity junction. Here, L is the lateral size of the periodic asperity and l_c is the horizontal projection of the contact length. This configuration generates a geometry characterized by 6 re-entrant corners (Fig. 3 (c)) which are a potential source of stress singularities and crack nucleation. Four re-entrant corners have an angle 2β, while the remaining two have an angle 2γ, being the two angles related by the equation $\beta = \pi/2 - \gamma$. The condition of adhesion between the two asperities is herein modelled by considering the two asperities as a monolithic solid, in line with theoretical arguments for complete contact problems in re[20, 23, 19]. The sliding motion of the asperities is simulated by imposing a horizontal displacement on the top and on the bottom of the unit asperity junction, see Fig. 3 (b).

Although the present mechanical problem is nonlinear, we know from [22] that the critical apparent shearing stress corresponding to crack propagation in the PF approach, which defines in the present problem the onset of debris formation, is ruled by a scaling of the type $T_c/L \sim \sqrt{EG_c/l}$, where T_c is the critical tangential force per unit out-of-plane thickness at debris formation, E and G_c are the Young's modulus and

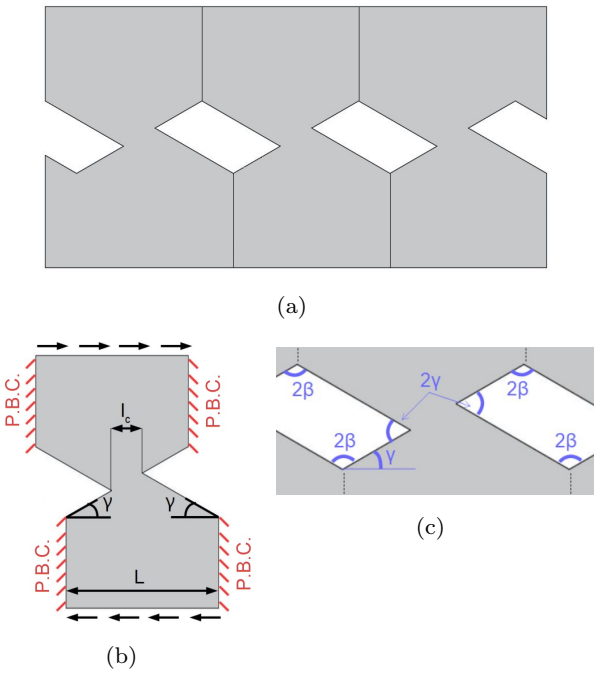

Fig. 3 Geometry of the computational model: (a) contact between periodically distributed asperities; (b) the unit asperity junction and the boundary conditions (dashes denote periodic boundary conditions while arrows denote imposed displacements); (c) the re-entrant corners present in the geometry.

the fracture toughness of the material, l is the internal length scale of the PF approach, and L is the lateral size of the asperity. Dimensional analysis suggests the following functional dependency in relation to the geometrical problem sketched in Fig.3:

$$T_c = T_c(E, G_c, l, L, l_c, \gamma), \tag{8}$$

which, after some manipulation leads to the following dimensionless form:

$$T_c^* = \frac{T_c}{L\sqrt{\dfrac{EG_c}{l}}} = \Phi\left(\frac{l_c}{L}, \gamma\right), \tag{9}$$

As a result, the dimensionless critical tangential force is expected to be function of just two parameters: l_c/L and γ.

In the following, a parametric analysis is carried out by varying three geometrical parameters: the asperity

Values of the geometrical parameters		
γ	15°; 30°; 45°; 60°; 75°	Asperity angle
L	1.0 ; 1.5 ; 2.0	Asperity lateral size (mm)
l_c	0.1 L ; 0.2 L ; 0.3 L ; 0.4 L	Horizontal projection of the junction area
Mechanical parameters		
E	117,000 MPa	Young modulus
v	0.35	Poisson ratio
G	70 N/mm	Fracture energy
l	0.2 mm	Phase Filed internal length scale

Table 1 Geometry and material parameters used in the simulation.

slope angle γ, the asperity size L, which is also the distance between two adjacent asperities, and the horizontal projection of the junction area l_c (Fig. 3 (b)). According to Eq. 9, the values selected for the parameters are collected in Table 1. This led to a total of 60 simulations, each one with around 57000 nodes. The choice of varying L in addition to l_c/L and γ is aimed at confirming the dimensional analysis results suggesting that the failure mode at crack nucleation is independent of L.

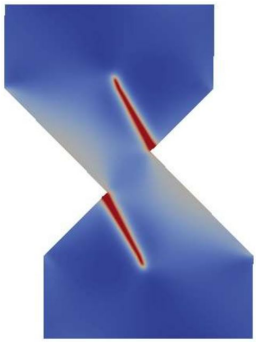

(a) Failure mode 1

(b) Failure mode 2

Fig. 4 Different failure modes observed from numerical test: (a) failure mode 1 corresponding to crack propagation from the re-entrant corner of amplitude 2γ; (b) failure mode 2 corresponding to crack propagation from the re-entrant corner of amplitude 2β.

3 Discussion of numerical results and mechanical interpretation

The numerical simulations show crack nucleation always in the proximity of a re-entrant corner. We distinguish between two failure modes: (1) crack propagation from the re-entrant corners of amplitude 2γ (Fig. 4 (a)); (2) crack propagation from the re-entrant corners of amplitude 2β (Fig. 4 (b)). Table 1 shows the prevailing failure mode (1 or 2) for each combination of the model parameters.

These results show that the failure mode is independent of the lateral size L, as expected from dimensional analysis considerations. Moreover, the dimensionless critical tangential force at the onset of crack growth is also almost independent of L, as highlighted in Fig. 5.

	$\gamma = 15°$			$\gamma = 30°$			$\gamma = 45°$			$\gamma = 60°$			$\gamma = 75°$		
	L			L			L			L			L		
l_c/L	1.0	1.5	2.0	1.0	1.5	2.0	1.0	1.5	2.0	1.0	1.5	2.0	1.0	1.5	2.0
0.1	1	1	1	1	1	1	1	1	1	1	1	1	2	2	2
0.2	1	1	1	1	1	1	1	1	1	2	2	2	2	2	2
0.3	1	1	1	1	1	1	1	1	1	2	2	2	2	2	2
0.4	1	1	1	1	1	1	1	1	1	2	2	2	2	2	2

Table 2 Crack nucleation (failure mode 1 or 2 based on Fig. 4) for each combination of model parameters.

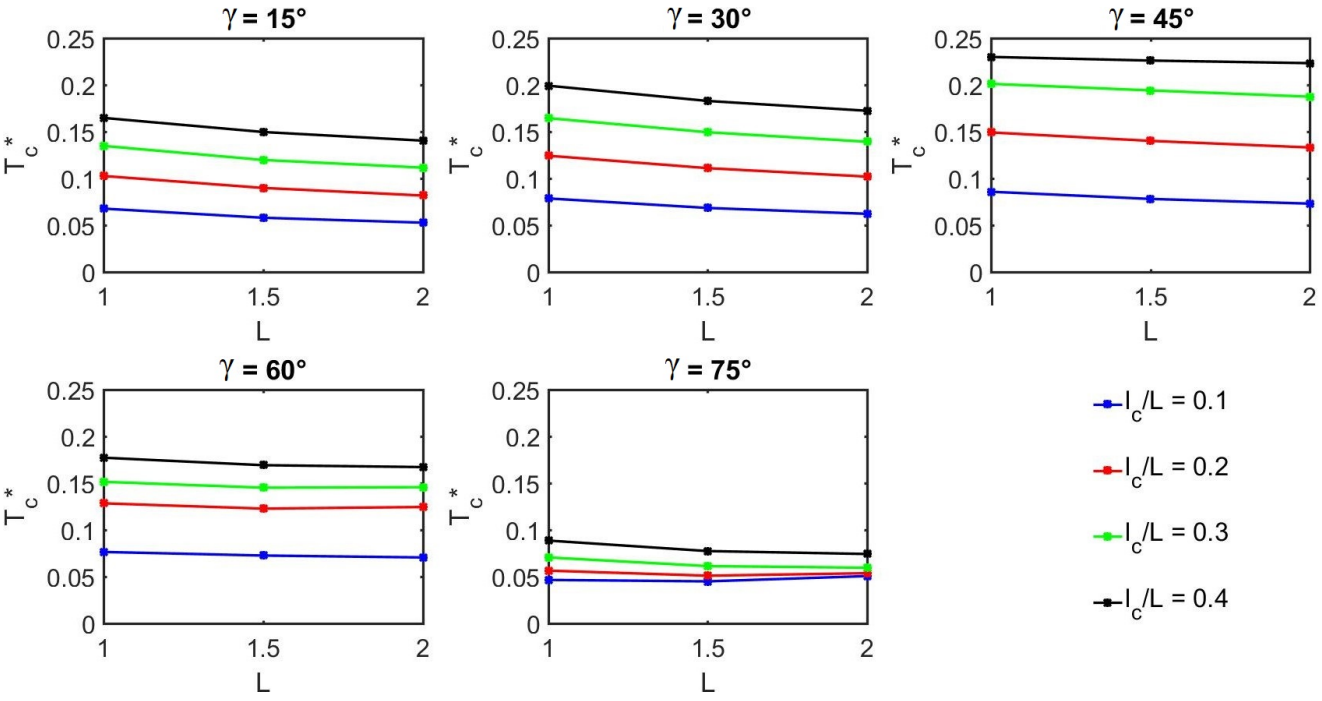

Fig. 5 Variation of T_c^* vs L for each combination of model parameter.

To propose a mechanical interpretation of the numerical results, we recall that the problem geometry presents 6 re-entrant corners (Fig. 3 (c)): 4 of amplitude 2β at the base of each asperity, and 2 of amplitude 2γ at the junction boundaries. Angles γ and β are complementary angles, i.e. $\beta + \gamma = \pi/2$. Those re-entrant corners can be the source for stress-singularities. Depending on their amplitudes, one stress singularity can prevail over the other, and it can lead to the failure mode 1 or 2. According to Linear Elastic Fracture Mechanics (LEFM), the stress-field components σ_{ij} near the tip of a re-entrant corner (at a radial distance $r \longrightarrow 0$) are given by the Williams asymptotic analysis [28]:

$$\sigma_{ij} = r^{\lambda-1} f_{ij}(\theta), \tag{10}$$

where r and θ are, respectively, the radial distance from the notch root and the angle measured from a horizontal axis emanating fro the notch tip (Fig. 6(a)), i and j are the indices identifying the components of the stress tensor, λ is the eigenvalue characterizing the power of the stress-singularity, and f is the corresponding eigenfunction [7,21]. For the present problem, the eigenvalues for Mode I and Mode II deformation, associated to notch opening or sliding, are given by the roots of the

following eigenequation:

$$\sin(2\lambda\alpha) \pm \lambda \sin(2\alpha) = 0, \tag{11}$$

where α is the angle shown in Fig. 6(a). The positive sign in Eq.(11) gives the roots corresponding to Mode I deformation (symmetric loading w.r.t. the angle bisector), while the negative eigenvalues sign gives the roots corresponding to Mode II deformation (antisymmetric loading), which is the loading condition relevant for the present problem. The solution of Eq.(11) is collected in [25], and is shown in Fig. 6(b) vs. β or γ ($0 \leq \beta, \gamma \leq \pi/2$).

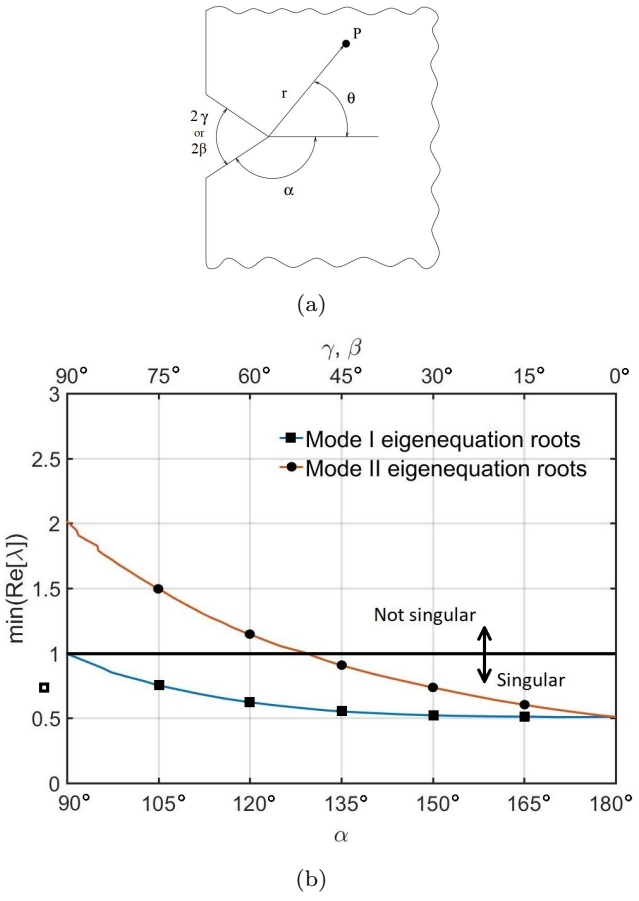

Fig. 6 (a) Re-entrant corner geometry and polar coordinates; (b) eigenvalue λ vs. α, γ and β.

As per Eq.(10), stress-singularities occur only for $\lambda < 1$. Consequently, considering the re-entrant corner angles in our numerical simulations, we can state the following simple criterion for the failure mode prediction: *the failure mode 1 with crack onset from the re-entrant corner of amplitude* 2γ *takes place if the associated power of the stress-singularities is higher than that corresponding to that of the re-entrant corner of amplitude* 2β*, while vice-versa for the failure mode 2.* The value of λ related to Mode II deformation for the angles γ and β tested in our simulations is collected in Table 3 for the various values of γ and β tested and those leading to a singular stress field (for γ or β less than 51°) are highlighted. The simulated failure mode is ruled by the most singular stress-singularity criterion as stated above. The only exception to such a rule occurs for $\gamma = 60°$ when both failure modes take place depending on the ratio l_c/L. Although the failure mode 2 should prevail according to the dominant stress-singularity criterion, failure mode 1 takes place for $l_c/L = 0.1$, which corresponds to re-entrant corner tips very close to each other. This exception can be explained by the elastic interactions between the two stress-singularities, which would need a refined analysis for the quantification.

4 Occurrence of steady-state wear

In this section we investigate the conditions leading to steady-state wear in our model junction problem. Steady state adhesive wear would happen when the new profile created by fracture has exactly the same geometry as that of the undeformed original one. Consequently, the invariance in the profile slope will reproduce exactly the same crack pattern up to infinity in the case of repeated tangential loadings. In order to investigate on this phenomenon, the angle γ' after fracture (estimated from the crack pattern) is compared to the originally underformed one, γ, and the quantity

Mode II stress-singularity				Crack onset based on numerical simulations	
γ	λ_γ	β	λ_β	Failure mode 1	Failure mode 2
15°	0.61	75°	1.50	X	
30°	0.74	60°	1.15	X	
45°	0.91	45°	0.91	X	
60°	1.15	30°	0.74	X	X
75°	1.50	15°	0.61		X

Table 3 Mode II eigenvalues of the stress-singularities for each simulated re-entrant corner. The eigenvalues which give a singular stress field are highlighted in blue. The symbol X denotes the occurrence of a given failure mode.

$\Delta\gamma = \gamma' - \gamma$ is used as a measure to quantify the deviation from the steady-state condition. This value is plotted vs. l_c/L in Fig. 7.

This plot further confirms the dimensional analysis results in Section 3 suggesting that the variation of $\Delta\gamma$ is mostly governed by the slope asperity angle γ and by l_c/L, while the lateral size L has a negligible effect. Fig. 4 shows the identified crack patterns from the simulation that closely reproduce the steady-state wear condition, i.e., those with $\gamma = 45°$.

5 Conclusions

In the present study, the problem of adhesive wear has been investigated in relation to periodic asperity junction models in the framework of the Archard interpretation suggesting that wear is the result of asperity fracture. Therefore, the Phase Field model for fracture has been exploited to simulate the crack pattern affecting the asperity junction model, depending on the size of the junction length, the lateral size of the asperity, and the amplitude of the re-entrant corner angles γ and β defined by the junction geometry. Results show that two failure modes are expected to occur, one with a crack nucleated at the re-entrant corner γ, and another with a crack nucleated at the re-entrant corner β. The occurrence of one failure mode over the other appears to be ruled, as a first glance, by a simple criterion based on the dominant stress-singularity at the two re-entrant corner tips. The reproducibility of the initial asperity junction geometry after debris formation due to crack growth can be used as a criterion to assess the occurrence of steady-state adhesive wear. From the numerical results we found that steady-state wear is likely to happen for $\gamma = 45°$, almost independently of the lateral size of the asperity and of the horizontal projection of the junction length.

Acknowledgements The authors would like to acknowledge Prof. D.A. Hills (University of Oxford) for useful discussion and suggestions on the problem of steady-state wear. JR acknowledges the support of the projects funded by the Spanish Ministry of Economy and Competitiveness/FEDER (Projects MAT2015-71036-P and MAT2015-71309-P) and the Andalusian Government (Projects of Excellence No. TEP-7093 and P12-TEP-1050).

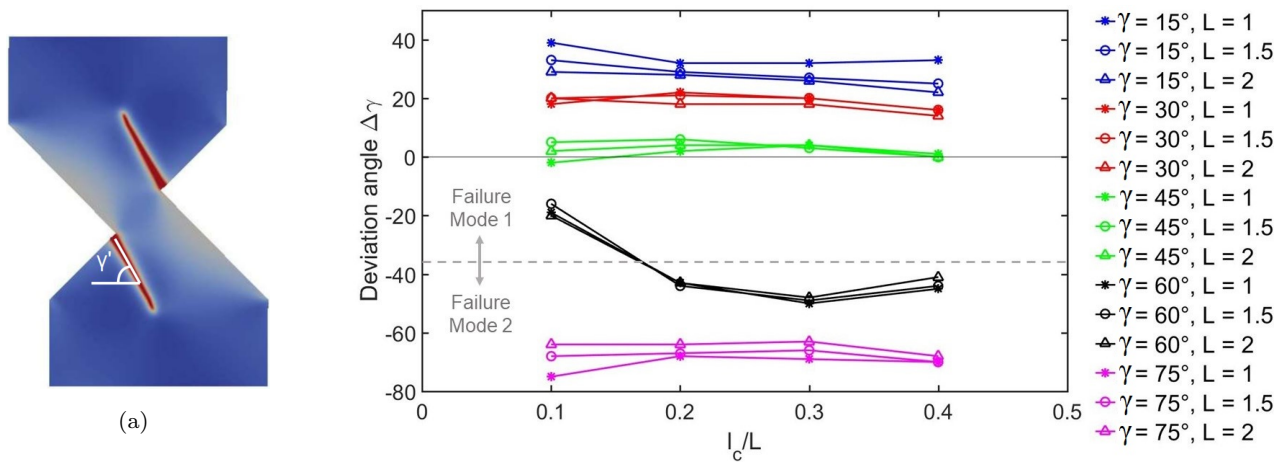

(a) (b)

Fig. 7 (a) Crack propagation angle γ'; (b) Deviation angle vs normalized contact area for all the simulations of the parametric analysis

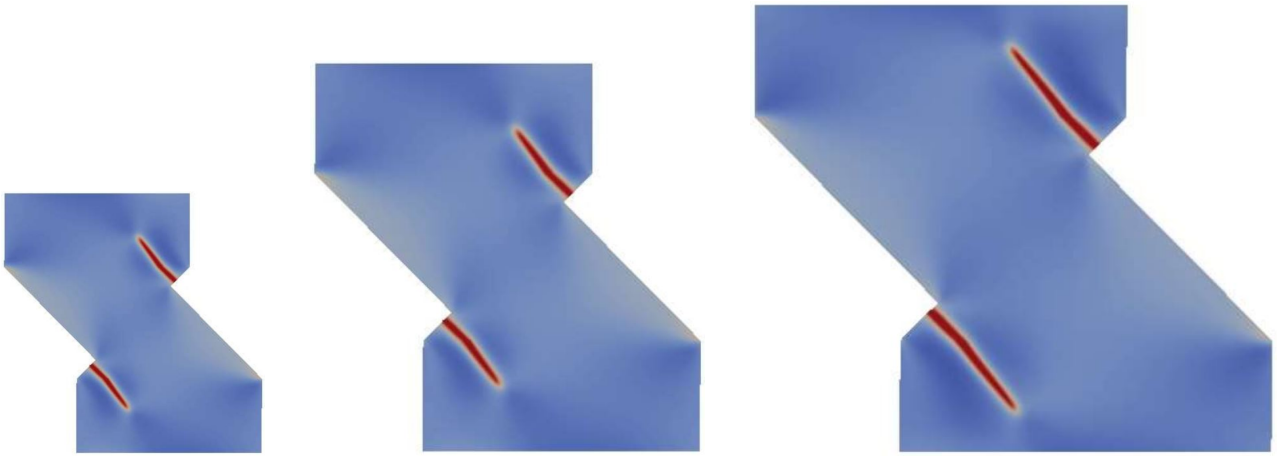

(a) $\gamma = 45°$, $L = 1.0$, $l_c = 0.4L$ (b) $\gamma = 45°$, $L = 1.5$, $l_c = 0.4L$ (c) $\gamma = 45°$, $L = 2.0$, $l_c = 0.4L$

References

1. Aghababaei, R., Warner, D.H., Molinari, J.F.: Critical length scale controls adhesive wear mechanisms. Nature communications **7** (2016)
2. Archard, J.: Contact and rubbing of flat surfaces. Journal of applied physics **24**(8), 981–988 (1953)
3. Bhushan, B.: Modern tribology handbook, two volume set. CRC press (2000)
4. Bourdin, B., Francfort, G.A., Marigo, J.J.: The variational approach to fracture. Journal of elasticity **91**(1), 5–148 (2008)
5. Brockley, C.A., Fleming, G.K.: A model junction study of severe metallic wear. Wear **8**(5), 374–380 (1965)
6. Buckley, D.H.: Surface effects in adhesion, friction, wear, and lubrication, vol. 5. Elsevier (1981)
7. Carpinteri, A., Paggi, M.: Analytical study of the singularities arising at multi-material interfaces in 2d linear elastic problems. Engineering fracture mechanics **74**(1), 59–74 (2007)
8. Chung, K.H., Kim, D.E.: Fundamental investigation of micro wear rate using an atomic force microscope. Tribology Letters **15**(2), 135–144 (2003)
9. Freddi, F., Royer-Carfagni, G.: Variational fracture mechanics to model compressive splitting of masonry-like

materials. Annals of Solid and Structural Mechanics **2**(2-4), 57–67 (2011)

10. Gotsmann, B., Lantz, M.A.: Atomistic wear in a single asperity sliding contact. Physical review letters **101**(12), 125501 (2008)
11. Greenwood, J.A., Tabor, D.: Deformation properties of friction junctions. Proceedings of the Physical Society. Section B **68**(9), 609 (1955)
12. Hills, D.A., Paynter, R.J.H., Nowell, D.: The effect of wear on nucleation of cracks at the edge of an almost complete contact. Wear **268**(7-8), 900–904 (2010)
13. Holm, R.: Electric contacts: theory and application. Springer Science & Business Media (2013)
14. Kayaba, T., Kato, K.: The analysis of adhesive wear mechanism by successive observations of the wear process in sem. Wear of Materials pp. 45–56 (1979)
15. Kim, H.K., Hills, D.A., Paynter, R.J.H.: Asymptotic analysis of an adhered complete contact between elastically dissimilar materials. The Journal of Strain Analysis for Engineering Design **49**(8), 607–617 (2014)
16. Lubarda, V.A., Krajcinovic, D., Mastilovic, S.: Damage model for brittle elastic solids with unequal tensile and compressive strengths. Engineering Fracture Mechanics **49**(5), 681–697 (1994)
17. Miehe, C., Hofacker, M., Welschinger, F.: A phase field model for rate-independent crack propagation: Robust algorithmic implementation based on operator splits. Computer Methods in Applied Mechanics and Engineering **199**(45), 2765–2778 (2010)
18. Miehe, C., Welschinger, F., Hofacker, M.: Thermodynamically consistent phase-field models of fracture: Variational principles and multi-field fe implementations. International Journal for Numerical Methods in Engineering **83**(10), 1273–1311 (2010)
19. Mugadu, A., Hills, D.A., Limmer, L.: An asymptotic approach to crack initiation in fretting fatigue of complete contacts. Journal of the Mechanics and Physics of Solids **50**(3), 531–547 (2002)
20. Mugadu, A., Hills, D.A., Nowell, D.: Modifications to a fretting-fatigue testing apparatus based upon an analysis of contact stresses at complete and nearly complete contacts. Wear **252**(5), 475–483 (2002)
21. Paggi, M., Carpinteri, A.: On the stress singularities at multimaterial interfaces and related analogies with fluid dynamics and diffusion. Applied Mechanics Reviews **61**(2), 020801 (2008)
22. Paggi, M., Reinoso, J.: Revisiting the problem of a crack impinging on an interface: a modeling framework for the interaction between the phase field approach for brittle fracture and the interface cohesive zone model. Computer Methods in Applied Mechanics and Engineering **321**, 145–172 (2017)
23. Porter, M.I., Hills, D.A.: Note on the complete contact between a flat rigid punch and an elastic layer attached to a dissimilar substrate. International journal of mechanical sciences **44**(3), 509–520 (2002)
24. Rabinowicz, E., Tanner, R.I.: Friction and wear of materials. Journal of Applied Mechanics **33**, 479 (1966)
25. Seweryn, A., Molski, K.: Elastic stress singularities and corresponding generalized stress intensity factors for angular corners under various boundary conditions. Engineering Fracture Mechanics **55**(4), 529–556 (1996)
26. Stachowiak, G., Batchelor, A.W.: Engineering tribology. Butterworth-Heinemann (2013)
27. Vahdat, V., Grierson, D.S., Turner, K.T., Carpick, R.W.: Mechanics of interaction and atomic-scale wear of amplitude modulation atomic force microscopy probes. ACS nano **7**(4), 3221–3235 (2013)
28. Williams, M.L.: Stress singularities resulting from various boundary conditions in angular corners of plates in extension. Journal of applied mechanics **19**(4), 526–528 (1952)
29. Zhong, J., Shakiba, R., Adams, J.B.: Molecular dynamics simulation of severe adhesive wear on a rough aluminum substrate. Journal of Physics D: Applied Physics **46**(5), 055307 (2013)
30. Zienkiewicz, O.C., Taylor, R.L.: The finite element method: solid mechanics, vol. 2. Butterworth-heinemann (2000)
31. Ziman, J.M.: Electrons in metals: A short guide to the fermi surface. Contemporary Physics **4**(2), 81–99 (1962)